Silicon-on-sapphire mid-IR wavefront engineering by using subwavelength grating metasurfaces

YUEWANG HUANG, QIANCHENG ZHAO, SALIH K. KALYONCU, RASUL TORUN, AND OZDAL BOYRAZ*

EECS Department, University of California, Irvine, California 92697, USA
*Corresponding author: oboyraz@uci.edu

Subwavelength high-contrast gratings (sub-λ HCGs) were pursued to design mid-IR optical devices based on wavefront engineering. Unlike metallic counterparts, dielectric and semiconductors offer low-loss operation over a wide spectral range. Silicon gratings on sapphire substrate are proposed here as the device platform due to their transparency at near-IR to mid-IR wavelengths. The proposed generic methodology manipulates the wavefront of the reflected wave based on the phase and magnitude of reflectivity for unit cells with different dimensions. To demonstrate the capability of generating an arbitrary wavefront profile, several design examples are shown: (1) a reflective mirror with $\sim$100% power efficiency and broad bandwidth of >1 µm as reflectivity $>90\%$; (2) a blazed grating with a reflection peak automatically aligned with its $+$1st diffraction order at 19.5°; (3) a focusing mirror with a focal length of 35 µm and diffraction-limited focus; (4) a sinusoidal phase profile with a periodicity of 8860 nm.   © 2016 Optical Society of America

OCIS codes: (050.2770) Gratings; (050.6624) Subwavelength structures; (130.3060) Infrared; (110.2760) Gradient-index lenses.

http://dx.doi.org/10.1364/JOSAB.33.000189

1. INTRODUCTION

Metasurfaces with engineered phase discontinuities are emerging as a new type of metamaterial that can be used to manipulate the phase and amplitude of electromagnetic waves [1–3]. In particular, metallic metasurfaces with plasmonic nanoantennas can provide wavefront shaping that is only possible by using multiple conventional optical components. However, metallic phase discontinuities often suffer from a narrowband operation window and high absorption loss. Alternatively, recent research on plasmonic metasurfaces shifts their attention to low-loss dielectric materials to overcome these limitations to deliver multifunctional optical surfaces [4,5]. Like many conventional components, a diffraction grating is one of the most widely used devices in modern optical systems with a wide range of varieties, e.g., blazed grating, concave grating, echelle grating, and holographic grating [6]. In conventional diffraction gratings, the grating period is often longer than the operating wavelength, hence leading to multiple diffraction orders in the transmission or reflection domain. Recently, gratings with periods smaller than the operating wavelength, known as subwavelength (sub-λ) gratings, have also been investigated intensively. Particularly, sub-λ high-contrast gratings (HCGs) with high refractive indices contrast when compared to the supporting substrate material are attracting special interest owing to the potential to support optical resonance in the medium [7]. When the grating dimensions are tuned properly to resonate

sub-λ HCGs can show ultrahigh reflection with $\sim$100% efficiency [8,9]. This property has been utilized to make high-performance reflective mirrors in forming resonance cavities in vertical-cavity surface-emitting lasers (VCSELs), quantum cascaded lasers, and high-Q optical resonators [9–12]. The reflectors could also be electrostatically actuated to achieve ultrashort wavelength tuning time in VCSELs [13]. Other applications based on sub-λ HCGs have also been demonstrated, including hollow-core waveguides, polarization splitters, and surface-enhanced Raman scattering [14–16]. In all these applications, the sub-λ HCGs are uniform with identical dimensions across the device and only the macroscopic high-reflectivity property is utilized. More interestingly, it has been recently discovered that the phase delay on the reflected wave is highly sensitive to the geometrical dimensions of the reflective sub-λ HCGs [17,18]. A variation of $>2\pi$ on the phase delay can be achieved by simply tuning the periodicity and duty cycle of the gratings. Hence, we can engineer the wavefront of the reflected wave by distributing sub-λ HCGs with different dimensions at different locations to generate an arbitrary wavefront profile. Based on this property, planar focusing reflectors based on sub-λ HCGs have been shown numerically and experimentally based on a silicon-on-insulator (SOS) platform [17,18]. It is also presented as a means of devising phase-discontinuity and composite metasurfaces [5,19]. Meanwhile, the phase property of sub-λ HCGs has also been utilized to redirect

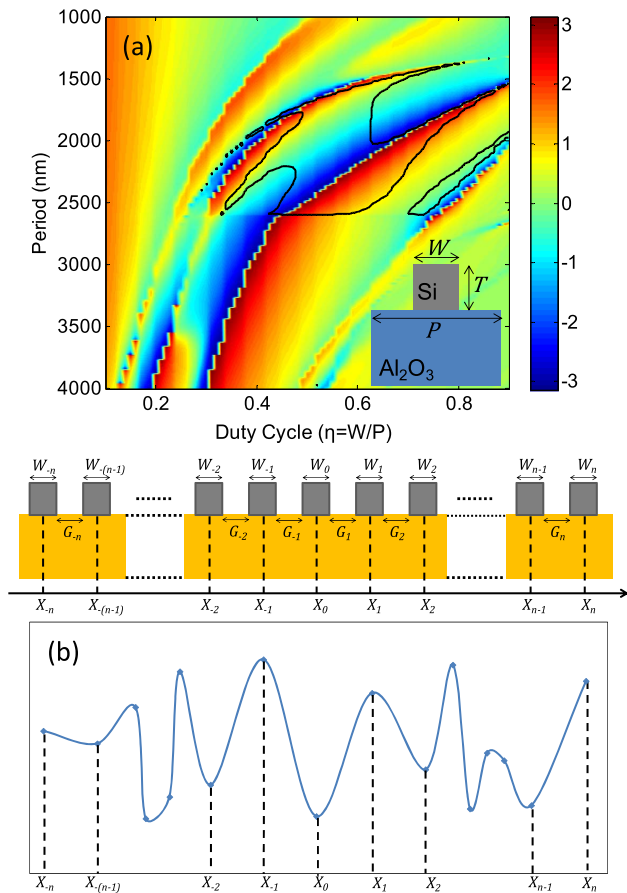**Fig. 1.** (a) Phase contour for silicon-on-sapphire grating cells with different grating periods and duty cycles at 4.3 µm mid-IR wavelength (TM polarized, grating thickness $T = 3.5$ µm). By changing the grating period and duty cycles, the phase difference on the reflected wave can be greater than 2π, while keeping the reflectivity greater than 90% (the region enclosed by black solid line). (b) Schematics of an example showing the design of an arbitrary wavefront profile. Grating parameters at each location X_i should be properly tuned to generate a phase corresponding to the function shown in the bottom of the figure.

better power efficiency. Another advantage of sub-λ HCGs for the mid-IR wavelength is that the critical dimension of the gratings is typically greater than 1 µm and conventional photolithography can be used to pattern the device relaxing the need of electron beam lithography or stepper shrinkage printing [28].

The paper is organized as follows. First, the generic design methodology is presented in Section 2. The design is approached by using a recursive search of geometrical parameters based on a lookup map [Fig. 1(a)] generated by parametric characterization of sub-λ HCG unit cells. Next, the simplest type of reflective mirror with a constant phase delay and ~100% power efficiency is presented in Section 3. The designed reflective mirror shows a broadband reflection with >90% efficiency over a bandwidth of more than 1 µm. We then applied the methodology to design a special type of blazed grating based on phase-gradient sub-λ HCG, in which the reflection peak will be self-aligned with the first diffraction order of the diffraction grating. Full-wave simulation is employed to verify that the expected design goals are achieved in good agreement with theoretical predictions. Another example is a quadratic phase profiler that is designed to facilitate an ideal focusing reflective mirror. Full-wave simulation was used to validate the designed focal length of 35 µm and 62% of the energy is confined within the ~2 µm radius spot at the focal point. In Section 6, a sinosoidal phase profiler is formed to show the capability of generating arbitary wavefront profiles in the sub-λ HCGs in the mid-IR spectrum.

2. DESIGN METHODOLOGY

Metasurfaces with phase discontinuities create reflected wave with spatially varying phase delay with respect to the incident wave. For the first step of the design, we determined the phase and amplitude response of SOS subwavelength gratings with different geometrical dimensions. SOS grating unit cells, shown in Fig. 1(a), were first simulated using the rigorous coupled wave analysis (RCWA) method [29]. Due to the subwavelength nature of the gratings, only the zeroth-order diffraction exists. Based on this, the original RCWA method was simplified by excluding higher-order diffractions in favor of simplicity and simulation speed. Here three parameters were explored, i.e., grating thickness (T), grating period (p), and grating duty cycle (DC). The phase delay of the reflected wave was a function of the grating thickness, grating period, and duty cycle, and was denoted as a function of T, p, and DC. Since the ultrahigh reflectivity in high-contrast subwavelength gratings is strongly related to the resonance effect in the grating grooves, the thickness of the gratings is essential to achieve high reflection efficiency in this type of subwavelength grating-based devices. By properly choosing the grating thickness, one can achieve a wide range of reflected phase $\phi(p, \text{DC})$ by tuning the grating period and duty cycles while maintaining a large reflectivity. As shown in Fig. 1(a), when the silicon grating thickness is chosen to be 3.5 µm, a reflected phase variation of >2π can be readily achieved within the region enclosed by the black solid line where the reflectivity is greater than 90%. With a manipulating range of >2π, we can theoretically design any phase profile by perturbing the geometrical parameters at different grating sites.

the propagation of waves to facilitate light coupling and mode conversion [20]. However, all these designs are dedicated in the visible and near-IR spectrum and no general design methodology is present. In this paper we proposed a general methodology for the design of arbitrary wavefront profiles in the mid-IR spectrum range. To exemplify the methodology, we demonstrate the design of a group of different grating devices including a conventional normal reflective mirror, a blazed grating, a focusing reflector, and a sinusoidal phase profiler at the mid-IR wavelength of 4.3 µm. A silicon grating on sapphire substrate was chosen as the platform due to the large index contrast between silicon and sapphire and the transparency of both materials in the mid-IR window [21–23]. The design procedure can further be manipulated to achieve multifunctional surfaces, such as reflectors, lenses, and polarization manipulators. Compared to another type of recent emerging wavefront engineering mechanism based on a plasmonic metasurface [2,24–27], sub-λ HCGs based on pure dielectric resonance have the advantage of the absence of ohmic loss and hence

Figure 1(b) illustrates an example of designing an arbitrary phase profile. Let us assume that the desired phase profile is an arbitrary function defined as $\phi(x) = f(x)$. Then the design procedure is to progressively and iteratively find (p_i, DC_i) pairs that satisfy the phase equation in Eq. (1), subject to the restriction of high reflectivity level to maintain high power efficiency. The recursion is programmed in Matlab using the precomputed reflectivity phase and magnitude obtained by the RCWA method:

$$\phi(x_i) = f\left(x_{i-1} + \frac{p_{i-1}}{2} + \frac{p_i}{2}\right) = \phi(p_i, DC_i). \qquad (1)$$

We seeded the recursion with a maximum reflectivity and then searched for the next pair of (p_i, DC_i) closest to (p_{i-1}, DC_{i-1}) which also meet the phase profile requirement in Eq. (1). In this way we can minimize the change between adjacent grating lines and improved matching to help the power efficiency of the designed devices.

3. DESIGN OF REFLECTIVE MIRRORS

First, we designed a simple high-efficiency reflective mirror. The phase delay function was constant across the whole region, namely,

$$\phi(x_i) = \phi(x_0). \qquad (2)$$

There was no complicated recursive for this simple phase profile; instead, we searched for the maximum reflectivity in order to achieve high power efficiency. Figure 2 shows the design of a uniform grating with a period of 1990 nm and duty cycle of 70%. Figure 2(a) shows the magnitude of the total magnetic field including both incident and scattered waves. There is negligible amplitude on the transmitted wave, and the standing wave pattern in the reflection domain reveals the total reflection nature. This phenomenon is due to the destructive interference of the two fundamental grating modes [7], manifesting itself as resonance in the grating layer shown in Fig. 2. Figure 2(b) shows the phase of only the scattered wave. The smaller phase periodicity in the substrate is the result of the higher refractive index of sapphire. Due to the subwavelength nature of this device, only the zeroth-order diffraction exists

and very high efficiency is expected. The simulated reflection efficiency is nearly 100% at a wavelength between 4.2 and 4.8 μm. The designed ideal reflective mirror is of broadband with a FWHM of >1 μm, as shown by the simulation results generated via both the RCWA method and the finite-element-method-based solver COMSOL Multiphysics in Fig. 2(c).

4. DESIGN OF BLAZED GRATING

Next, we show the design of a blazed grating using subwavelength gratings. Here we designed a special type of blazed grating which automatically aligns its peak transmission with the first diffraction order [27,30]. In this grating, each period consists of six subwavelength patches with different dimensions. It was designed so that there is 2π phase shift within each period. Therefore, the phase profile for a blazed grating has a quasi-linear phase gradient along the x direction as expressed by Eq. (3),

$$\phi(x_i) = \phi(x_0) - \frac{2\pi}{\Lambda} x_i, \qquad (3)$$

where Λ is the periodicity of the supercell consisting of subgratings with different geometrical parameters. There is a constant phase gradient along the x direction that equals $(\nabla\phi)_x = \frac{2\pi}{\Lambda}$. If the incidence is normal, the reflected wave will have a tangential wave vector component of $k_x = (\nabla\phi)_x$. Therefore, the reflected angle θ_r will be theoretically determined by

$$k_0 \sin\theta_r = k_x. \qquad (4)$$

In this design we targeted a periodicity of $\Lambda = 13$ μm. Theoretically we should have the peak reflection at $\sin^{-1}(k_x/k_0) = \sin^{-1}(\lambda/\Lambda) = 19.3°$. In addition, according to the Bragg's Law, we have the grating equation

$$\Lambda(\sin\theta_i + \sin\theta_m) = m\lambda. \qquad (5)$$

For normal incidence, we have

$$\Lambda \sin\theta_m = m\lambda. \qquad (6)$$

Thus, we have the +1st order diffraction at $\theta_{+1} = \sin^{-1}(\lambda/\Lambda)$, which is the same as the peak transmission direction of the designed blazed grating. Therefore, the first-order diffraction is self-aligned with the peak transmission,
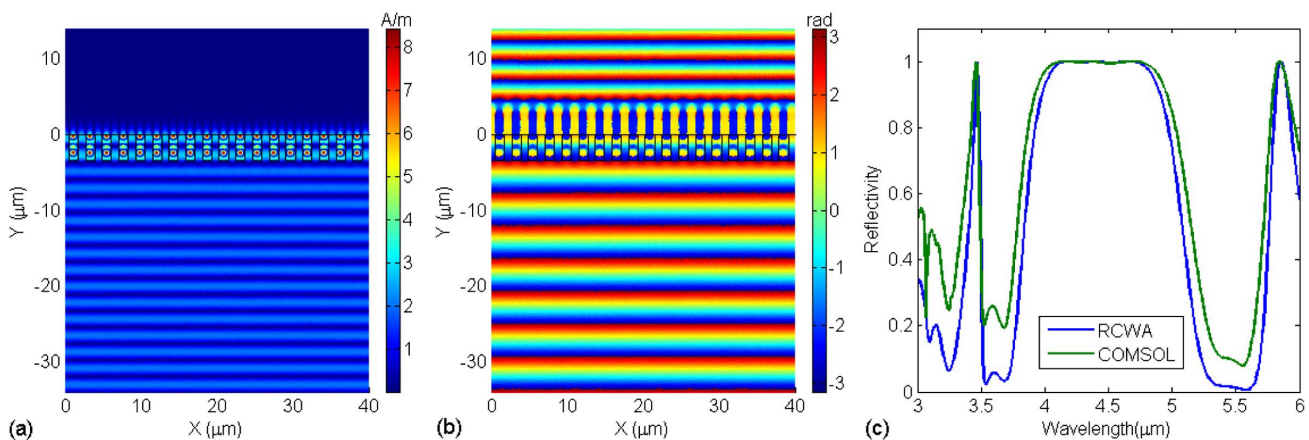

Fig. 2. Simulation results of the designed subwavelength grating as a high power efficiency reflective mirror: (a) total magnetic field of both incident and reflected wave; (b) phase of only the scattered wave; (c) performance of the mirror at different wavelengths.
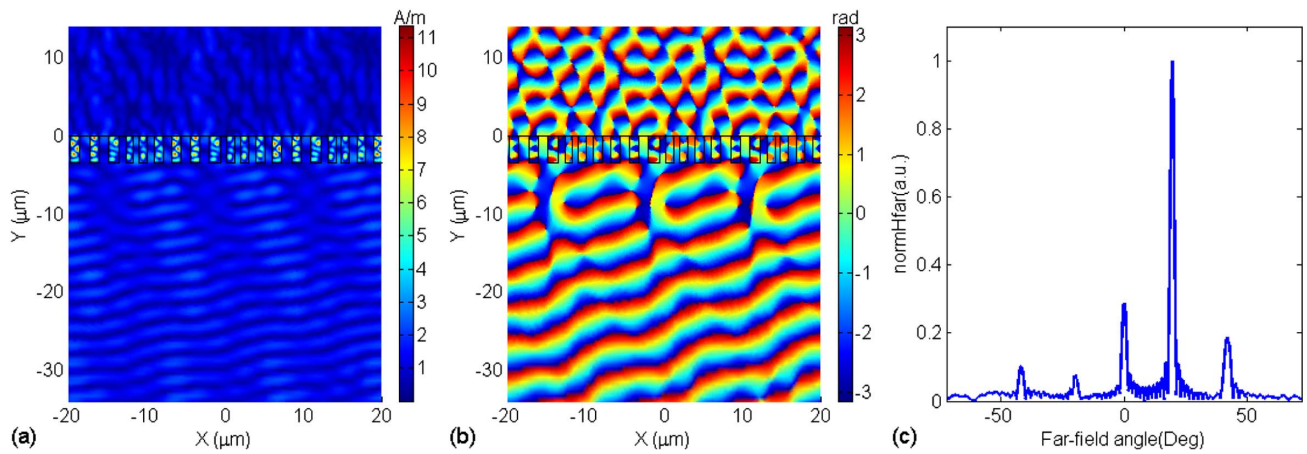
Fig. 3. (a) Magnitude and (b) phase of the blazed grating under normal TM-polarized incidence from the bottom; (c) far-field radiation of the reflected field to different angles.
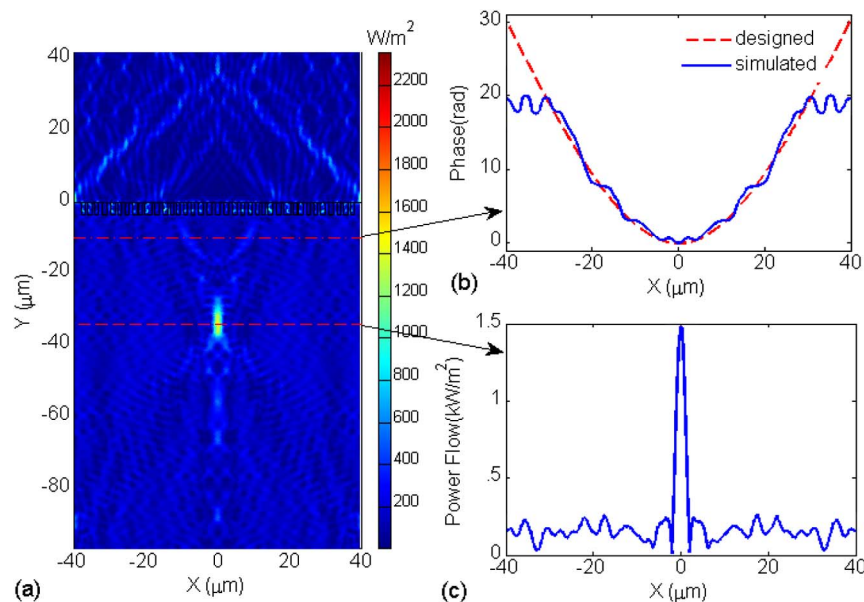

Fig. 4. (a) Full-wave power flow magnitude for the designed focusing reflector; (b) phase profile along the dashed line; (c) power flow distribution along the bottom dashed line through the focal point.

which is the desired design objective in the blazed grating design. In order to verify the design, we also simulated the designed structure using full-wave simulation based on the finite-element method. Figure 3 shows the simulated result of the designed blazed grating with six grating subcells in each supercell repeating in the x direction. Figure 3(a) illustrates the interference pattern of the reflected wave and incident wave, which reveals the oblique reflection in the device. Figure 3(b) exhibits the phase of only the scattered field. It is clear that the wavefront of the reflected wave propagates toward an angle to the right. To characterize this angled reflection, the far-field pattern of the design was calculated and illustrated in Fig. 3(c). The first-order diffraction falls to an angle of 19.5°, which agrees well with the theoretical prediction. Meanwhile, higher-order reflections are also

present. The theoretical power efficiency of the blazed grating is shown aside. This far-field radiation pattern also agrees with the theoretical diffraction efficiency. Unlike conventional blazed gratings, the designed blazed grating is flat because all the subgratings in the device have the same height. This is highly desirable for nanophotonic integration.

5. DESIGN OF FOCUSING MIRRORS

The third example demonstrates the design of a focusing reflector. The wavefront phase profile of an ideal focusing reflector is defined by Eq. (7) and all reflected waves will have constructive interference at the focal point. We use the stated design methodology to design the device,

$$\phi(x_i) = \phi(x_0) + \frac{2\pi}{\lambda}\left(\sqrt{F^2 + x_i^2} - F\right), \qquad (7)$$

where F is the designed focal length. Figure 4 shows the full-wave simulation result of a design with $F = 35$ μm. Figure 4(b) shows the phase of the reflected wave at the red dashed-dotted line located 10 μm away from the reflector surface along with the theoretical phase defined by Eq. (7) at the same distance. It is clear that a nearly quadratic phase profile is indeed generated, closely resembling the desired phase profile, except for the margin of the device due to nonideal boundary conditions. Figure 4(c) shows the power flow on the cut-plane at the focal spot, as denoted by the red dashed line. The simulated field plot clearly shows the focusing of energy to a distance of ∼35 μm. Defraction-limited focus is achieved and 62% of the energy is confined within the ∼2 μm radius spot. Further optimization may still improve the power efficiency. Weakened focus can also be observed at the transmission side due to the electromagnetic duality.

6. DESIGN OF A SINUSOIDAL PHASE PROFILE

While we demonstrated the capability of the generic method by designing several functional devices common in the optics domain, many other applications (e.g., hologram image encoding, vortex wave plates, and simultaneous manipulation of field and polarization) require more complex wavefront engineering [31–34]. To further demonstrate the ability of arbitrary wavefront profile generation, we hereby show the design of a more complicated sinusoidal phase profile. The target wavefront can be denoted by the function in Eq. (8). Here, Λ is the periodicity of the sinusoidal function, which was chosen to be 8860 nm in this example. Figures 5(a) and 5(b) show the simulated magnitude and phase of the magnetic field using COMSOL. Figure 5(c) shows the phase of the reflected wave at the location along the red line. The phase profile closely resembles the designed target sinusoidal shape. This design case demonstrates the capability of generating an arbitrary
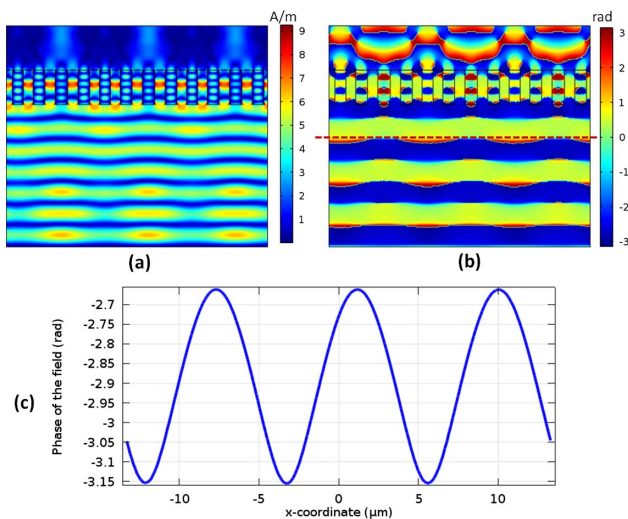
wavefront profile using the proposed methodology. With this generic approach, a wide range of functional devices can be designed in the mid-IR range with high power efficiency:

$$\phi(x_i) = \phi(x_0) - A\sin\left(\frac{2\pi}{\Lambda}x_i\right). \qquad (8)$$

7. SUMMARY

We explored the opportunities of optoelectronic devices based on subwavelength high-index-contrast gratings (sub-λ HCGs) at the mid-IR spectrum. High reflectivity and large reflected phase delay variation can be simultaneously achieved in properly designed sub-λ HCGs. This property can be utilized to engineer the wavefront of the electromagnetic wave to design various optical devices based on wavefront forming. A generic design methodology was proposed based on the parametric simulation resulting in sub-λ HCG cells using the RCWA method. An arbitrary wavefront profile can be generated theoretically. To demonstrate this capability, we realized this method to design different optical devices based on sub-λ HCGs. First, a high-efficiency reflective mirror was designed. Almost 100% efficiency was achieved at the designed wavelength with an observed broad band of >1 μm for the designed mirror. Next, we designed a special blazed grating, whose diffraction peak would be self-aligned to the +1st diffraction order with periodicity of 13 μm and with peak diffraction falling to an angle of 19.5°. A focusing mirror with a quadratic wavefront profile was then designed with full-wave simulation to validate the designed focal length of 35 μm and 62% of the energy was confined within the ∼2 μm radius spot at the focal point. Finally, a sinosoidal phase profile is formed to show the capability of generating complex wavefront profiles in the sub-λ HCGs in the mid-IR spectrum. All the design examples demonstrated the proposal design method. With this methodology, a wide variety of mid-IR devices can be designed using sub-λ HCGs.

REFERENCES

1. V. M. Shalaev, "Optical negative-index metamaterials," Nat. Photonics **1**, 41–48 (2007).
2. A. V. Kildishev, A. Boltasseva, and V. M. Shalaev, "Planar photonics with metasurfaces," Science **339**, 1232009 (2013).
3. N. Yu and F. Capasso, "Flat optics with designer metasurfaces," Nat. Mater. **13**, 139–150 (2014).
4. Y. Yang, I. I. Kravchenko, D. P. Briggs, and J. Valentine, "All-dielectric metasurface analogue of electromagnetically induced transparency," Nat. Commun. **5**, 5753 (2014).
5. D. Lin, P. Fan, E. Hasman, and M. L. Brongersma, "Dielectric gradient metasurface optical elements," Science **345**, 298–302 (2014).
6. J. M. Lerner, J. Flamand, J. P. Laude, G. Passereau, and A. Thevenon, "Diffraction gratings ruled and holographic—A review," Proc. SPIE **0240**, 82–89 (1981).
7. V. Karagodsky, F. G. Sedgwick, and C. J. Chang-Hasnain, "Theoretical analysis of subwavelength high contrast grating reflectors," Opt. Express **18**, 16973–16988 (2010).
8. C. F. R. Mateus, M. C. Y. Huang, L. Chen, C. J. Chang-Hasnain, and Y. Suzuki, "Broad-band mirror (1.12-1.62 μm) using a subwavelength grating," IEEE Photonics Technol. Lett. **16**, 1676–1678 (2004).

Fig. 5. (a) Magnitude and (b) phase of the magnetic field, and (c) the phase of the reflected wave at the location denoted by the red line.

9. C. J. Chang-Hasnain and W. Yang, "High-contrast gratings for integrated optoelectronics," Adv. Opt. Photonics **4**, 379–440 (2012).

10. W. Hofmann, C. Chase, M. Muller, Y. Rao, C. Grasse, G. Böhm, M.-C. Amann, and C. J. Chang-Hasnain, "Long-wavelength high-contrast grating vertical-cavity surface-emitting laser," IEEE Photonics J. **2**, 415–422 (2010).

11. S. Boutami, B. Benbakir, J.-L. Leclercq, and P. Viktorovitch, "Compact and polarization controlled 1.55 μm vertical-cavity surface-emitting laser using single-layer photonic crystal mirror," Appl. Phys. Lett. **91**, 071105 (2007).

12. F. Brückner, D. Friedrich, T. Clausnitzer, M. Britzger, O. Burmeister, K. Danzmann, E.-B. Kley, A. Tünnermann, and R. Schnabel, "Realization of a monolithic high-reflectivity cavity mirror from a single silicon crystal," Phys. Rev. Lett. **104**, 163903 (2010).

13. Y. Zhou, M. C. Huang, and C. J. Chang-Hasnain, "Tunable VCSEL with ultra-thin high contrast grating for high-speed tuning," Opt. Express **16**, 14221–14226 (2008).

14. Y. Zhou, V. Karagodsky, B. Pesala, F. G. Sedgwick, and C. J. Chang-Hasnain, "A novel ultra-low loss hollow-core waveguide using subwavelength high-contrast gratings," Opt. Express **17**, 1508–1517 (2009).

15. J. Feng, C. Zhou, J. Zheng, H. Cao, and P. Lv, "Dual-function beam splitter of a subwavelength fused-silica grating," Appl. Opt. **48**, 2697–2701 (2009).

16. X. Deng, G. B. Braun, S. Liu, P. F. Sciortino, B. Koefer, T. Tombler, and M. Moskovits, "Single-order, subwavelength resonant nanograting as a uniformly hot substrate for surface-enhanced Raman spectroscopy," Nano Lett. **10**, 1780–1786 (2010).

17. F. Lu, F. G. Sedgwick, V. Karagodsky, C. Chase, and C. J. Chang-Hasnain, "Planar high-numerical-aperture low-loss focusing reflectors and lenses using subwavelength high contrast gratings," Opt. Express **18**, 12606–12614 (2010).

18. D. Fattal, J. Li, Z. Peng, M. Fiorentino, and R. G. Beausoleil, "Flat dielectric grating reflectors with focusing abilities," Nat. Photonics **4**, 466–470 (2010).

19. Y. Yang, W. Wang, P. Moitra, I. I. Kravchenko, D. P. Briggs, and J. Valentine, "Dielectric meta-reflect array for broadband linear polarization conversion and optical vortex generation," Nano Lett. **14**, 1394–1399 (2014).

20. P. Cheben, D.-X. Xu, S. Janz, and A. Densmore, "Subwavelength waveguide grating for mode conversion and light coupling in integrated optics," Opt. Express **14**, 4695–4702 (2006).

21. Y. Huang, E. K. Tien, S. Gao, S. K. Kalyoncu, Q. Song, F. Qian, E. Adas, D. Yildirim, and O. Boyraz, "Electrical signal-to-noise ratio improvement in indirect detection of mid-IR signals by wavelength conversion in silicon-on-sapphire waveguides," Appl. Phys. Lett. **99**, 181122 (2011).

22. R. A. Soref, S. J. Emelett, and W. R. Buchwald, "Silicon waveguided components for the long-wave infrared region," J. Opt. Pure Appl. Opt. **8**, 840–848 (2006).

23. Y. Huang, E.-K. Tien, S. Gao, S. K. Kalyoncu, Q. Song, F. Qian, and O. Boyraz, "Quasi-phase matching in SOI and SOS based parametric wavelength converters," Proc. SPIE **8120**, 81200F (2011).

24. F. Aieta, P. Genevet, M. A. Kats, N. Yu, R. Blanchard, Z. Gaburro, and F. Capasso, "Aberration-free ultrathin flat lenses and axicons at telecom wavelengths based on plasmonic metasurfaces," Nano Lett. **12**, 4932–4936 (2012).

25. Y. Huang, Q. Zhao, S. K. Kalyoncu, R. Torun, Y. Lu, F. Capolino, and O. Boyraz, "Plasmonic sub-wavelength phase-gradient metasurfaces for real time dispersive imaging," in *CLEO*, OSA Technical Digest (online) (Optical Society of America, 2014), p. STu1M.7.

26. A. Pors, O. Albrektsen, I. P. Radko, and S. I. Bozhevolnyi, "Gap plasmon-based metasurfaces for total control of reflected light," Sci. Rep. **3**, 2155 (2013).

27. Y. Huang, Q. Zhao, S. K. Kalyoncu, R. Torun, Y. Lu, F. Capolino, and O. Boyraz, "Phase-gradient gap-plasmon metasurface based blazed grating for real time dispersive imaging," Appl. Phys. Lett. **104**, 161106 (2014).

28. Y. Huang, Q. Zhao, S. K. Kalyoncu, R. Torun, Y. Lu, and O. Boyraz, "Silicon on sapphire mid-IR wave-front engineering by using subwavelength gratings," in *CLEO*, OSA Technical Digest (online) (Optical Society of America, 2014), p. FW1K.5.

29. M. G. Moharam and T. K. Gaylord, "Rigorous coupled-wave analysis of planar-grating diffraction," J. Opt. Soc. Am. **71**, 811–818 (1981).

30. S. Sun, K.-Y. Yang, C.-M. Wang, T.-K. Juan, W. T. Chen, C. Y. Liao, Q. He, S. Xiao, W.-T. Kung, G.-Y. Guo, L. Zhou, and D. P. Tsai, "High-efficiency broadband anomalous reflection by gradient metasurfaces," Nano Lett. **12**, 6223–6229 (2012).

31. W. T. Chen, K.-Y. Yang, C.-M. Wang, Y.-W. Huang, G. Sun, I.-D. Chiang, C. Y. Liao, W.-L. Hsu, H. T. Lin, S. Sun, L. Zhou, A. Q. Liu, and D. P. Tsai, "High-efficiency broadband meta-hologram with polarization-controlled dual images," Nano Lett. **14**, 225–230 (2014).

32. X. Ni, A. V. Kildishev, and V. M. Shalaev, "Metasurface holograms for visible light," Nat. Commun. **4**, 2807 (2013).

33. P. Genevet, N. Yu, F. Aieta, J. Lin, M. A. Kats, R. Blanchard, M. O. Scully, Z. Gaburro, and F. Capasso, "Ultra-thin plasmonic optical vortex plate based on phase discontinuities," Appl. Phys. Lett. **100**, 013101 (2012).

34. M. Veysi, C. Guclu, O. Boyraz, and F. Capolino, "Thin anisotropic metasurfaces for simultaneous light focusing and polarization manipulation," J. Opt. Soc. Am. B **32**, 318–323 (2015).